Inorganic Chemistry

Article

pubs.acs.org/IC

Sr_2FeO_3 with Stacked Infinite Chains of FeO_4 Square Planes

Cédric Tassel,[†,‡] Liis Seinberg,[†] Naoaki Hayashi,[‡] Subodh Ganesanpotti,[†] Yoshitami Ajiro,[§] Yoji Kobayashi,[†] and Hiroshi Kageyama*[,†,∥]

[†]Department of Energy and Hydrocarbon Chemistry, Graduate School of Engineering, Kyoto University, Nishikyo-ku, Kyoto 615-8510, Japan

[‡]The Hakubi Center for Advanced Research, Kyoto University, Yoshida-Ushinomiya-cho, Sakyo-ku, Kyoto 606-8302, Japan

[§]Graduate School of Human and Environmental Studies, Kyoto University, Kyoto 606-8501, Japan

[∥]CREST, Japan Science and Technology Agency (JST), Kawaguchi Center Building 4-1-8, Honcho, Kawaguchi, Saitama 332-0012, Japan

Supporting Information

ABSTRACT: The synthesis of Sr_2FeO_3 through a hydride reduction of the Ruddlesden–Popper layered perovskite Sr_2FeO_4 is reported. Rietveld refinements using synchrotron and neutron powder diffraction data revealed that the structure contains corner-shared FeO_4 square-planar chains running along the [010] axis, being isostructural with Sr_2CuO_3 (*Immm* space group). Fairly strong Fe–O–Fe and Fe–Fe interactions along [010] and [100], respectively, make it an $S = 2$ quasi two-dimensional (2D) rectangular lattice antiferromagnet. This compound represents the end-member ($n = 1$) of the serial system $Sr_{n+1}Fe_nO_{2n+1}$, together with previously reported $Sr_3Fe_2O_5$ ($n = 2$) and $SrFeO_2$ ($n = \infty$), thus giving an opportunity to study the 2D-to-3D dimensional crossover. Neutron diffraction and Mössbauer spectroscopy show the occurrence of *G*-type antiferromagnetic order below 179 K, which is, because of dimensional reduction, significantly lower than those of the other members, 296 K in $Sr_3Fe_2O_5$ and 468 K in $SrFeO_2$. However, the temperature dependence of magnetic moment shows a universal behavior.

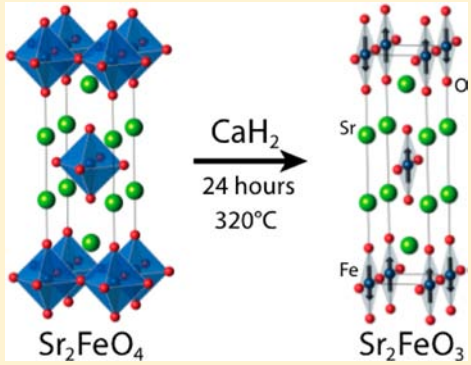

INTRODUCTION

One-dimensional (1D) antiferromagnetic (AF) systems have attracted much attention because of their numerous properties such as the spin-Peierls distortion for $S = {}^1/_2$ chains[1] and a spin-singlet formation by hidden symmetry breaking in $S = 1$ (Haldane) chains.[2] Two-dimensional (2D) AF systems have also been intensively investigated, with quantum and frustration effects being discovered that include a quantum disordered state in triangular and Kagomé lattices,[3] and quantized magnetization plateaus in a Shastry–Sutherland lattice.[4]

Given these successes in understanding the magnetism of both 1D and 2D systems, the next step is to learn the relationship between the two systems. Such a study can be achieved with intermediate dimensional structures that allow one to observe dimensional crossover. In fact, after the discovery of high-T_c superconducting cuprates, $S = {}^1/_2$ *n*-legged spin ladders (where n = integer) were proposed theoretically to understand the relation between the 2D AF square lattice and the 1D AF chain.[5] Interestingly, the 1D magnetism is not connected smoothly to the 2D case; a gapless magnetic state is expected for n = odd, while a spin-singlet state with a finite energy in the spin excitation spectrum is expected for n = even. This prediction was validated experimentally through a series of $S = {}^1/_2$ spin ladder compounds $Sr_{n-1}Cu_nO_{2n+1}$, $SrCu_2O_3$ ($n = 2$), $Sr_2Cu_3O_5$ ($n = 3$), and $SrCuO_2$ ($n = \infty$), obtained by high pressure and high temperature synthesis.[6]

We have recently reported iron oxides $SrFeO_2$ and $Sr_3Fe_2O_5$ with Fe in square planar coordination, synthesized by a low temperature hydride reduction of $SrFeO_3$ and $Sr_3Fe_2O_7$.[7] $SrFeO_2$ and $Sr_3Fe_2O_5$ exhibit *G*-type magnetic order at relatively high temperatures of T_N = 468 and 296 K, respectively. Here, the precursors belong to the $n = \infty$ and $n = 2$ members of the Ruddlesden–Popper type layered perovskite family $Sr_{n+1}Fe_nO_{3n+1}$ ($n = 1, 2, 3,\ldots \infty$). Therefore, we may assume that a homologous series of $Sr_{n+1}Fe_nO_{2n+1}$ ($n = 1, 2, 3,\ldots \infty$) is obtained by the hydride reduction of $Sr_{n+1}Fe_nO_{3n+1}$:

$$Sr_{n+1}Fe^{4+}{}_nO_{3n+1} + CaH_2 \rightarrow Sr_{n+1}Fe^{2+}{}_nO_{2n+1} + CaO + H_2 \quad (1)$$

Regarding magnetic interactions, we originally addressed that $Sr_{n+1}Fe_nO_{2n+1}$ can be regarded as the $S = 2$ version of serial *n*-legged spin ladders', as illustrated in Figure 1 of ref 7b. This was based on the assumption that the in-plane Fe–O–Fe superexchange interaction ($J_\parallel$) is predominant. However, density functional theory (DFT) calculations on $SrFeO_2$[8] and

Received: February 20, 2013
Published: May 8, 2013

   dx.doi.org/10.1021/ic400444u | Inorg. Chem. 2013, 52, 6096–6102

$Sr_3Fe_2O_5$[9] revealed that the out-of-plane Fe−Fe direct exchange interaction ($J_\perp$) between face-to-face FeO_4 square planes is not at all negligible. $J_\parallel$ = 7.91 meV and $J_\perp$ = 2.29 meV[8] and $J_\parallel$ = 6.58 meV and $J_\perp$ = 1.75 meV[9] were obtained, giving the $J_\perp/J_\parallel$ ratio of around 0.3. This result was later confirmed experimentally by inelastic neutron scattering experiments for $SrFeO_2$.[10] These observations have changed our view of the $Sr_{n+1}Fe_nO_{2n+1}$ system and it is now better regarded as an S = 2 intermediate dimensional system that connects a 2D rectangle lattice with a 3D cuboid lattice, as illustrated in Figure 1.

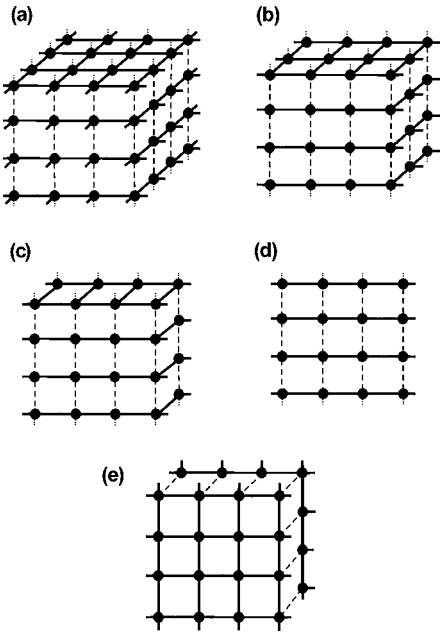

Figure 1. (a)−(d) Magnetic interactions between metal centers in $Sr_{n+1}Fe_nO_{2n+1}$. $SrFeO_2$ ($n = \infty$) (a), hypothetical $Sr_4Fe_3O_7$ (n = 3) (b), $Sr_3Fe_2O_5$ (n = 2) (c), and Sr_2FeO_3 (n = 1) (d). Solid and dotted lines, respectively, represent $J_\parallel$ and $J_\perp$. (e) The magnetic interactions in $Sr_3Fe_2O_4Cl_2$.

$SrFeO_2$ ($n = \infty$) is the terminal compound for the 3D side, and $Sr_3Fe_2O_5$ (n = 2) is the intermediate dimensional phase closer to the 2D extreme. Here, we report on the synthesis of Sr_2FeO_3, the n = 1 phase as the 2D terminal phase. This new phase is isostructural with Sr_2CuO_3[11] and contains stacked chains of corner shared FeO_4 square planes. We compare the structure, chemical and magnetic properties of this material with that of the other members of the series.

EXPERIMENTAL SECTION

Synthesis. Stoichiometric amounts of powders of Fe_2O_3, obtained from the decomposition of FeO(OH), and $Sr(OH)_2{\cdot}8H_2O$ were mixed thoroughly in air in an agate mortar, and heated under flowing oxygen gas for 6 h at 700 °C. Annealing Sr_2FeO_4 at higher temperatures led to its decomposition into $Sr_3Fe_2O_{7-x}$. This heating condition hinders the use of more conventional $SrCO_3$ because of its poor reactivity. The obtained Sr_2FeO_4 was checked by X-ray diffraction (XRD) using a Bruker D8 Advance diffractometer. The Sr_2FeO_4 specimen contained a small amount of $SrCO_3$. Sr_2FeO_4 and CaH_2 (99.9%) were mixed with a 1:2 molar ratio in an Ar-filled glovebox. The mixture was pelletized and sealed in evacuated Pyrex tubes (volume 15 cm^3) with pressure less than 1.3×10^{-2} Pa and then heated in a muffle furnace at 280 °C for 96 h. The resulting mixture contained a new phase, unreacted CaH_2 and byproducts such as CaO and $SrCO_3$ according to XRD analysis. Several attempts to eliminate CaH_2 and CaO, for example, by washing with a solution of 0.1 M of NH_4Cl in dried methanol in an Ar-filled glovebox, were unsuccessful, resulting in decomposition of the new phase. Thus, all analyses were performed using the multiphased specimen.

Synchrotron Powder XRD. The powder synchrotron XRD (SXRD) experiments were performed at room temperature (r.t.) on the large Debye−Scherrer camera installed at the Japan Synchrotron Radiation Research Institute SPring-8 BL02B2 by using an imaging plate as a detector. Incident beams from a bending magnet were monochromatized to 0.77709 Å. The powder sample was sieved to a 32 μm mesh and sealed in a Pyrex capillary with an inner diameter of 0.2 mm in an Ar-filled glovebox. The data were collected in a 2θ range from 0° to 75° with a step interval of 0.01°.

Neutron Powder Diffraction. Neutron powder diffraction (NPD) data were obtained at 9 and 180 K on the Kinken powder diffractometer for high efficiency high resolution measurements with multicounters, HERMES, of the Institute for Materials Research (IMR), Tohoku University, installed at the guide hall of the JRR-3 reactor in the Japan Atomic Energy Agency (JAEA), Tokai. The incident neutron with a wavelength of 1.82646 Å was monochromatized by the 331 reflection of a Ge crystal. A 12′-blank-sample-18′ collimation was employed. A polycrystalline sample of 5 g mass was placed into a vanadium cylinder, which was sealed under He atmosphere by an indium wire. Data were collected with a step-scan procedure (a step width of 0.1°) using 150 ^{3}He neutron detectors arranged in a 2θ range from 3° to 153°.

Structural Refinement. The crystal (and magnetic) structures were refined using synchrotron X-ray and neutron diffraction data. The powder Rietveld method, implemented in the computer programs JANA2006[12] and RIETAN-FP,[13] was used. The peak shape model used was a modified split-pseudo-Voigt function. The agreement indices are the R-weighted pattern factor, $R_{wp} = [\sum w_i(y_{io} - y_{ic})^2/\sum w_i(y_{io})^2]^{1/2}$, R-pattern, $R_p = \sum|y_{io} - y_{ic}|/\sum(y_{io})$, R-Bragg factor, $R_I = \sum|I_o(h_k) - I(h_k)|/\sum I_o(h_k)$ and goodness of fit (GOF), $\chi^2 = [R_{wp}/R_{exp}]^2$, where $R_{exp} = [(N - P)/\sum w_i y_{io}^2]^{1/2}$, y_{io} and y_{ic} are the observed and calculated intensities, w_i is the weighting factor, $I_o(h_k)$ and $I(h_k)$ are the observed and calculated integrated intensities, N is the total number of y_{io} data when the background is refined, and P is the number of adjusted parameters. The bond valence sum (BVS) method was applied to estimate the valence of cations using tabulated parameters, $r_0(Fe^{2+}-O^{2-})$ = 1.734 Å and $r_0(Sr^{2+}-O^{2-})$ = 2.118 Å.[14]

Mössbauer Spectroscopy. The Mössbauer spectra of Sr_2FeO_3 at room and low temperatures were taken under a dynamical vacuum, and the data were collected in transmission geometry by using a ^{57}Co/Rh γ-ray source in combination with a constant-acceleration spectrometer. The source velocity was calibrated by using pure α-Fe. The obtained spectra were fitted by a Lorentzian function.

RESULTS

Synthesis. Laboratory XRD (Supporting Information, Figure S1) showed the successful synthesis of the precursor phase Sr_2FeO_4 with the $I4/mmm$ space group. The cell parameters of $a \sim 3.86$ Å and $c \sim 12.41$ Å agree well with those previously reported.[15] The precursor phase contains a tiny amount of $SrCO_3$, which might be due to slight variation of the water content in $Sr(OH)_2{\cdot}8H_2O$. The reduced phase, obtained at 280 °C with a reaction time of 96 h, is highly unstable in air. Without a washing step, the final product contains unreacted calcium hydride and calcium oxide byproduct, together with strontium carbonate. Additionally, a small amount of strontium oxide possibly resulting from the collapse of Sr_2FeO_4 upon reduction was observed in diffraction patterns. Iron-containing impurities were not found in XRD nor Mössbauer spectroscopy (Figure 3). The new phase collapses rapidly upon exposure to air, in contrast to $SrFeO_2$ that is stable and $Sr_3Fe_2O_5$ that decomposes very slowly (a complete decomposition takes several days). Ruddlesden−Popper type perovskite phases are

dx.doi.org/10.1021/ic400444u | Inorg. Chem. 2013, 52, 6096−6102

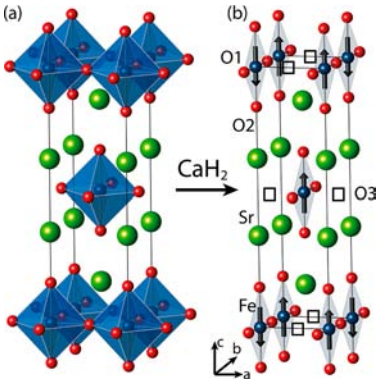

Figure 2. Crystallographic structures of Sr_2FeO_4 (a) and its reduced phase, Sr_2FeO_3 (b). Blue, red, and green balls represent iron, oxygen, and strontium, respectively. The squares represent the vacant (O3) site. Arrows in (b) indicate the spin moments on iron showing the *G*-type order below T_N.

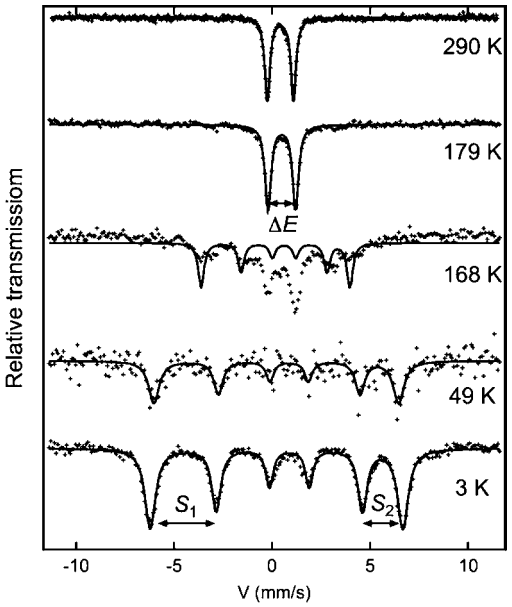

Figure 3. ^{57}Fe Mössbauer spectra of Sr_2FeO_3 at various temperatures. Dots and solid lines represent the observed and calculated fit, respectively. S_1 and S_2 correspond, respectively, to the split between the first and second peaks and that between the fifth and sixth peaks. ΔE is the quadrupole splitting in the paramagnetic phase.

known for their ability to intercalate water to some extent, as seen in $Sr_3NdFe_3O_{9-\delta}$ that converts into $Sr_3NdFe_3O_{7.5}(OH)_2{\cdot}H_2O$.[16] Therefore, the air-sensitivity of the $Sr_{n+1}Fe_nO_{2n+1}$ structure, an intergrowth structure of square-planar blocks and rock-salt blocks, appears to be strongly related to the number density of rock-salt SrO layers per unit volume.

Structural Refinement. The SXRD profile of the new structure can be indexed with an *I*-centered orthorhombic lattice with $a \sim 3.55$ Å, $b \sim 3.92$ Å, and $c \sim 12.93$ Å. The comparison of the obtained lattice parameters with those of the initial tetragonal compound Sr_2FeO_4 indicates a substantial shortening of the *a* axis by 0.4 Å. Such anisotropic shortening has been previously observed for both $SrFeO_2$ (along the *c* axis)[7a] and $Sr_3Fe_2O_5$ (along the *a* axis),[7b] suggesting the complete removal of the bridging apical oxygen atoms along the [100] direction in the present case. Mössbauer spectroscopy at r.t. (Figure 3) showed a sharp doublet indicating that iron is in a single site. A divalent high-spin state in FeO_4 square-planar coordination is derived from the observed isomer shift of ~4.2 mm/s and the quadrupole splitting (*QS*) of 1.332 mm/s. These values are close to those obtained for the $n = 2$ and $n = \infty$ phases.[7,8]

From the SXRD and Mössbauer results, it is naturally assumed that the reduced phase crystallizes in the Sr_2CuO_3 structure (Figure 2b) which is described in the *Immm* space group with similar lattice parameters, $a = 3.485$ Å, $b = 3.912$ Å, and $c = 12.688$ Å.[15] Rietveld refinement of SXRD data was performed using the aforementioned structure; Sr was placed on the 4*i* site (0, 0, *z*), Fe on 2*a* (0, 0, 0), and O on two different sites 2*d* (0, 0.5, 0) and 4*i* (0, 0, *z*). $SrCO_3$, CaO, CaH_2, and SrO, observed as impurity phases, were added to the calculation. The refinement (Figure 4) converged to a

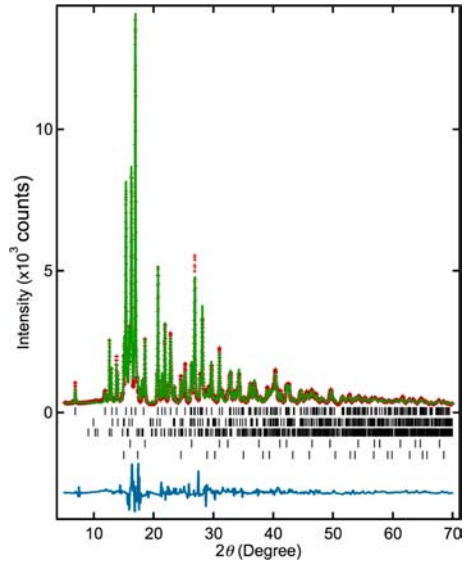

Figure 4. Structural characterization of Sr_2FeO_3 by Rietveld refinement of synchrotron XRD at 293 K. Red crosses, green solid line, and blue solid line stand for the observed, calculated, and difference intensities, respectively. Black ticks indicate the position of the calculated Bragg reflections of, from up to down, Sr_2FeO_3, CaH_2, $SrCO_3$, CaO, and SrO.

reasonable fit with $R_{wp} = 9.74\%$ and $\chi^2 = 2.51$ (Table 1). The occupation factors *g* of the oxygen sites were checked and we obtained $g_{O1} = 1.068(2)$, $g_{O2} = 1.054(1)$. This led to the conclusion that both O1 and O2 sites are fully occupied. We also checked the fractional occupancy of the supposedly vacant site at 2*b* (O3) (see Figure 2b) between face-to-face FeO_4 square planes.

When g_{O3} was allowed to change, we obtained $g_{O3} = -0.06(1)$, confirming that the apical oxygen atoms in Sr_2FeO_4 along the *a* axis are completely absent. From this the new material was found to have a Sr_2FeO_3 stoichiometry. The final refinement was therefore performed assuming full occupancy for O1 and O2 and zero occupancy for O3. The quantities of impurity phases in weight percent are 9.80% for $SrCO_3$, 1.10% for SrO, 14.97% for CaH_2, and 13.52% for CaO (Supporting Information, Figure S2). The calculated bond valences for Fe, Sr, O1, and O2 were +2.05, +1.79, −2.10, and −1.77, respectively. These values are similar to those expected for divalent iron, strontium, and oxygen and are comparable with

dx.doi.org/10.1021/ic400444u | Inorg. Chem. 2013, 52, 6096−6102

Table 1. Refined Structural Parameters of Sr_2FeO_3 Obtained from Neutron (9 and 190 K) and Synchrotron Powder Diffraction (293 K)[a]

atom	site		9 K	190 K	293 K
Sr	4*i*	*x*	0	0	0
		y	0	0	0
		z	0.3534(3)	0.3532(5)	0.3506(1)
		U_{iso} (100 Å^2)	0.013(7)	0.27(9)	0.23(3)
Fe	2*a*	*x*	0	0	0
		y	0	0	0
		z	0	0	0
		U_{iso} (100 Å^2)	0.10(1)	1.3(1)	0.68(6)
		μ_B	3.2		
O1	2*d*	*x*	0	0	0
		y	0.5	0.5	0.5
		z	0	0	0
		U_{iso} (100 Å^2)	0.10(1)	1.5(2)	1.0(2)
O2	4*i*	*x*	0	0	0
		y	0	0	0
		z	0.1589(3)	0.1582(6)	0.1547(3)
		U_{iso} (100 Å^2)	0.014(9)	0.77(16)	1.25*
		R_{wp}(%)	5.06	7.24	9.74
		R_p(%)	3.91	5.67	7.24
		R_b(%)	1.79	3.01	6.71
		χ^2	2.02	1.77	2.51
		a	3.5337(9)	3.5397(11)	3.5510(1)
		b	3.9095(9)	3.9138(12)	3.9216(1)
		c	12.9123(12)	12.9296(17)	12.9336(4)

[a]The value annoted with * was fixed.

Table 2. Comparison of the Calculated BVS of Iron and Strontium at 293 K for $Sr_3Fe_2O_5$,[8] Sr_2FeO_3, and $SrFeO_2$.[7]

$Sr_3Fe_2O_5$		Sr_2FeO_3		$SrFeO_2$	
Fe	1.95	Fe	2.06	Fe	1.97
Sr1	1.87	Sr	1.79	Sr	1.92
Sr2	1.87	O1	2.10	O	1.95
O1	1.90	O2	1.77		
O2	2.04				
O3	1.77				

the previously reported values for $Sr_3Fe_2O_5$ and $SrFeO_2$ (Table 2).

The analysis of NPD pattern of Sr_2FeO_3 at 190 K showed consistent tetragonal parameters and peak extinctions with the SXRD pattern. The structural parameters obtained by aforementioned synchrotron refinement were used along with the impurity phases of $SrCO_3$, SrO, CaO, and CaH_2. The fit provided reasonable agreement values of R_{wp} = 7.24% and χ^2 = 1.77. The occupancy factors for the O1, O2, and O3 sites are g_{O1} = 1.01(2), g_{O2} = 1.00(1), and g_{O3} = −0.01(1), confirming again that O1 and O2 are fully occupied, while O3 is completely vacant. The impurity amounts were 6.6% for $SrCO_3$, 3.0% for SrO, 6.3% for CaH_2, and 17.4% for CaO (Supporting Information, Figure S3). Note here that different batches were used for SXRD and NPD experiments.

Microstructure. The high-intensity and high-resolution diffraction pattern obtained from synchrotron X-rays allowed us to observe significant anisotropic broadening for (*h*0*l*) and (0*kl*) reflections in the newly formed lattice. As shown in Supporting Information, Table S1, the full width at half-maximum (*fwhm*) for the (013) and (103) peaks are 0.146° at 15.35° and 0.177° at 16.25°, respectively. We observed as well values of 0.159° for the (110) peak at 16.92° and 0.107° for the (004) peak at 20.7°. In general, *fwhm* increases at wider angles. This anomalous evolution of *fwhm* implies large anisotropic broadening, possibly due to disorder or strain along particular directions like [100] and [010], induced during the topochemical structural transformation. To accurately fit the profile of Sr_2FeO_3, the Stephens model of anisotropic broadening[17] was employed as implemented in JANA2006. The expression used for modeling the microstrain broadening is

$$\sigma^2(M_{hkl}) = \sum_{HKL} S_{HKL} h^H k^K l^L \tag{2}$$

$$\frac{1}{d^2} = M_{HKL} \tag{3}$$

where σ is the standard deviation of a Bragg peak that is directly correlated to its *fwhm*. The S_{HKL} terms are defined for $H + K + L = 4$, so that, for instance, the *fwhm* of (*h*00) peaks depends on the S_{400} parameter and the (*hk*0) peaks on the S_{220}, S_{400}, and S_{040} parameters. For our orthorhombic structure, the refined parameters were S_{400}, S_{040}, S_{004}, S_{220}, S_{202}, and S_{022}. Here, if S_{400} is large, it implies that all peaks with $h \neq 0$ contain broadening induced by defects or strain along the *a* axis. The agreement values before the use of this model were R_{wp} = 11.2% and χ^2 = 2.9. We found that S_{400} = 44.1, S_{040} = 13.6, and S_{220} = −6.1 and the other parameters were rounded off to zero. When the model was applied, the agreement values decreased to R_{wp} = 9.74% and χ^2 = 2.52. The large positive values of S_{400} and S_{040} are consistent with the observed broadening, respectively, for (*h*0*l*) and (0*kl*). The negative value of S_{220} compensates the large values obtained for S_{400} and S_{040} and is in agreement with sharp (*hh*0) peaks (vs (*h*0*l*) and (0*kl*) peaks). To summarize, the presence of defects or strains is important along [100] and [010], while it is negligibly small along [001] and [110].

Magnetic Properties. The NPD pattern at 9 K revealed the presence of additional reflections (Figures 5 and S4),

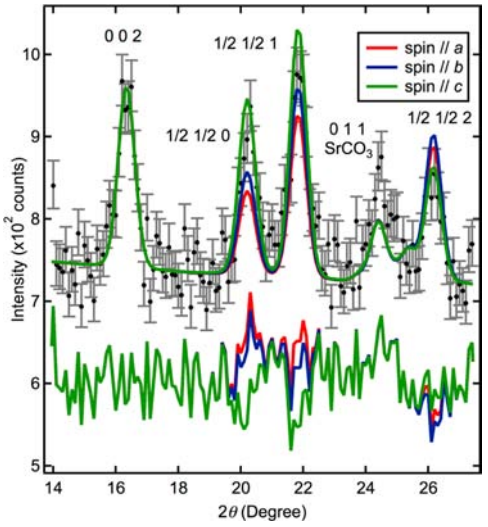

Figure 5. Comparison of the Rietveld refinement of the magnetic structure with the spin aligned parallel with the *a* (red), *b* (blue), and *c* (green) axis of the Sr_2FeO_3 structure. Note: The $SrCO_3$ peak was already observed before reduction (Supporting Information, Figure S1).

dx.doi.org/10.1021/ic400444u | Inorg. Chem. 2013, 52, 6096−6102

indicating a long-range magnetic order. These peaks were described with a propagation vector of (π, π, 0). The nuclear and magnetic structure at 9 K was refined with the $P1$ space group and an enlarged cell that is related to the crystal structure by $2a \times 2b \times c$ unit cell. We assumed the G-type spin order as found in Sr_2FeO_4.[18] To determine the spin orientation, we conducted the refinement of the magnetic structure assuming spin directions along the a, b, or c axis. The results are compared in Figure 5. The best agreement was obtained for the ($^1/_2$, $^1/_2$, 0) and ($^1/_2$, $^1/_2$, 1) reflections when the spins are aligned along the c axis. The reliability index, R_B, is 2.08%, which is better than 2.52% and 2.36% when aligned along the a- and b-axis orientation. The same c-axis spin orientation is observed in $Sr_3Fe_2O_5$. Thus the final Rietveld refinement with the selected spin orientation gave a good fit as shown in Table 1 and Figure 6. The magnetic moment at 9 K was refined to

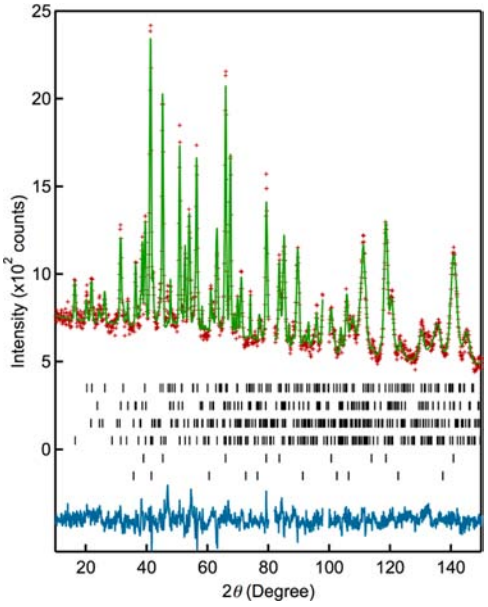

Figure 6. Structural characterization of Sr_2FeO_3 by Rietveld refinement of neutron diffraction at 9 K. Red crosses, green solid line, and blue solid line stand for the observed, calculated, and difference intensities, respectively. Black ticks indicate the position of the calculated Bragg reflections of, from up to down, the Sr_2FeO_3 chemical peaks, the Sr_2FeO_3 magnetic peaks, CaH_2, $SrCO_3$, CaO, and SrO. The angle range 80−82° and 98−100° contained peaks from an unknown phase and were removed from the fit.

yield 3.1(1) μ_B/Fe, which is smaller than the theoretically expected value for divalent, high spin state $S = 2$, but coherent with the previously reported values for $SrFeO_2$ (3.6 μ_B at 10 K)[7a] and $Sr_3Fe_2O_5$ (2.76 μ_B at 10 K).[7b]

Figure 3 shows the Mössbauer spectra of Sr_2FeO_3 at different temperatures. A doublet in the 290 and 179 K spectra indicates a paramagnetic state. The 168 K spectrum indicates the occurrence of long-range magnetic order, and the Néel temperature T_N should be between 168 and 179 K. With lowering temperature, the hyperfine field (HF) increases and reaches ~39 T at 3 K, which indicates the $S = 2$ state for iron, as also shown by NPD.

In $SrFeO_2$, the electric field gradient (EFG) at the iron site is perpendicular to the square plane by its site symmetry D_{4h}.[7a] In $Sr_3Fe_2O_5$ and the present compound Sr_2FeO_3, the FeO_4 square planar coordination is distorted only slightly and has similar EFG values at room temperature, indicating that the EFG should be almost parallel to the a axis. Figure 3 shows the width $S_1 - S_2$ is ~1.3 mm/s at 3 K, which is close to the room-temperature EFG value. This observation demonstrates that the magnetic moments lie perpendicular to the a axis, which is consistent with the NPD result.

DISCUSSION

Structural Evolution during the Reaction. The hydride reduction of Sr_2FeO_4 containing FeO_6 octahedral coordination at low temperature (<400 °C) results in the stoichiometric phase Sr_2FeO_3 ($n = 1$) with chains of corner-shared FeO_4 square planar coordination. The reaction condition is similar to other hydride-reduced ferrous structures, for example, $CaFeO_2$ (280 °C)[19] and $Sr_3Fe_2O_4Cl_2$ (350 °C),[20] showing a general trend that the oxygen extraction from iron perovskite-based frameworks is effective even at low temperatures.[7c] The general reaction to yield a series of square-planar coordinate iron oxides from corresponding Ruddlesden−Popper perovskite oxides with octahedral coordination is written as (1). For $n = \infty$ and 2, however, this reaction formula is an oversimplified and misleading description because $SrFeO_2$ and $Sr_3Fe_2O_5$ are not directly transformed from $SrFeO_3$ and $Sr_3Fe_2O_7$, respectively.[7a,b] Upon reduction of $SrFeO_3$, its composition continuously changes until it reaches $SrFeO_{2.5}$ with Fe^{3+} in tetrahedral and octahedral coordination geometries, and then $SrFe^{3+}O_{2.5}$ is directly converted to $SrFeO_2$ without nonstoichiometric intermediates. Likewise, upon reduction of $Sr_3Fe_2O_7$, its composition continuously changes until it becomes $Sr_3Fe^{3+}{}_2O_6$ with Fe^{3+} in square pyramidal coordination geometry. By further reduction, $Sr_3Fe_2O_6$ is directly converted to $Sr_3Fe_2O_5$ without nonstoichiometric intermediates. In contrast, the reaction to yield Sr_2FeO_3 is likely to occur without any Fe^{3+} containing $Sr_2FeO_{4-\delta}$ intermediate structures. No intermediate phases such as $Sr_2FeO_{3.5}$ were observed in the diffraction data. Here, Fe^{4+} with octahedral coordination converts directly to Fe^{2+} in square-planar coordination. Thus, the structural conversion in the present system is much simpler.

Microstructure analysis gives us a hint to understand the reaction pathway. Typically, if anisotropic broadening does not exist with strains being homogeneous in all the directions of the material, S_{HKL} values would be null. When S_{HKL} is large, disorder or strain exists within the HKL direction and negative S_{HKL} show specifically unstrained directions.

The observation of a naught value for S_{004} indicates that there are only negligible strains along the c direction, when Sr_2FeO_3 is transformed to Sr_2FeO_4 by low temperature reduction. The positive values of S_{400} and S_{040} can be explained by the modifications of the ab plane during the tetragonal to orthorhombic symmetry change. The formation of chains in two directions from the tetragonal Sr_2FeO_4 generates a "twinning" effect with respect to the ab plane in Sr_2FeO_3. This inevitably creates defects along the d_{100} and d_{010} directions that is translated into the broadening of the $h \neq 0$ and $k \neq 0$ hkl peaks. The very large value of S_{400} compared with S_{040} can be explained by the large d_{100} change (8.7%) during reduction against +1.5% for d_{010}. The value of S_{220} is slightly negative, which might be due to compensation of the overly positive S_{400} and S_{040} values.

The negligible changes occurring within the 00l planes in addition to the full occupancy of the O2 site indicate that apical oxygen atoms stay still during the reaction, confining the oxygen migration path within the perovskite-based layer.

dx.doi.org/10.1021/ic400444u | Inorg. Chem. 2013, 52, 6096−6102

Similar S parameters have been observed for $LaSrCoO_3H_{0.7}$ formed during the CaH_2 reaction of $LaSrCoO_4$.[21] The structure of $LaSrCoO_3H_{0.7}$ is similar to Sr_2FeO_3 but contains H^- anions between CoO_4 square planes.

Magnetic Properties. Concerning the local structure around iron, the FeO_4 square plane in Sr_2FeO_3 is stretched only slightly along the c axis: d_{Fe-O2} = 2.001 Å and d_{Fe-O1} = 1.961 Å (Table 3). A similar distortion is observed in $Sr_3Fe_2O_5$

Table 3. Comparison of the Calculated Bond Length (in Å) of Iron and Strontium at r.t. for the $Sr_{1+n}Fe_nO_{2n+1}$ series

Sr_3FeO_5		Sr_2FeO_3		$SrFeO_2$	
Fe−O1	1.976	Fe-Ol	1.961	Fe−O	1.995
Fe−O2	2.039	Fe−O2	2.001		
Fe−O3	2.013				
Sr1−O1	2.601	Si−Ol	2.624	Sr−O	2.646
Sr1−O2(1)	2.648	Si−O2(l)	2.646		
Srl−O2(2)	2.48	Si−O2(2)	2.534		
Sr2−O1	2.667				
Sr2−O3	2.645				

with Fe−O distances of 2.039 Å and 2.013 Å along the c axis and 1.976 Å along the b axis. The proximity of the local structure and chemical bonding in this series of iron oxides promises systematic and comparative discussion on the dimensional reduction from 3D and 2D in terms of magnetism.

In $Sr_3Fe_2O_5$, there are two in-plane Fe−O−Fe interactions, $J_{\|}$(leg) along the b axis and $J_{\|}$(rung) along the c axis. However, since the FeO_4 plane is only slightly deformed from the ideal square plane in $SrFeO_2$, we can assume that $J_{\|}$(leg) and $J_{\|}$(rung) are close to each other and to $J_{\|}$ for $SrFeO_2$. Theoretical calculations are indeed consistent with this expectation, providing $J_{\|}$(leg) = 6.37 meV and $J_{\|}$(rung) = 6.07 meV. Likewise, owing to the slight distortion of FeO_4 square plane in Sr_2FeO_3, the in-plane Fe−O−Fe interaction along the b axis should be close to those for $SrFeO_2$ and $Sr_3Fe_2O_5$. We can also assume that the out-of-plane Fe−Fe interactions $J_\perp$ are comparable in these three compounds because of similar distances between the facing FeO_4 square planes. $J_\perp$ = 1.48 is obtained theoretically for $Sr_3Fe_2O_5$[9] giving a $J_\perp/J_{\|} \sim 0.25$ ratio similar with that of the infinite layer compound. The interchain and interladder interactions in Sr_2FeO_3 and $Sr_3Fe_2O_5$, respectively, are negligible since they are spatially separated, requiring bended Fe−O−O−Fe super-superexchange pathways. Furthermore, these interactions are "effectively" canceled out because of geometrical frustration caused by the I-lattice cell (see Supporting Information, Figure S5).

There are two dominant magnetic interactions in $Sr_{n+1}Fe_nO_{2n+1}$, the superexchange interaction $J_\perp$ and the direct exchange interaction $J_{\|}$ ($J_\perp < J_{\|}$). $Sr_{n+1}Fe_nO_{2n+1}$ (n = integer) is a serial intermediate dimensional system that connects the 3D anisotropic lattice ($SrFeO_2$) with the 2D anisotropic square lattice (Sr_2FeO_3). Reflecting the dimensional reduction from 3D ($n = \infty$) to 2D (n = 1) through an intermediate dimension (n = 2). The magnetic order in Sr_2FeO_3 is significantly reduced; T_N ~179 K of Sr_2FeO_3 is much lower than 296 K in $Sr_3Fe_2O_5$ and 468 K in $SrFeO_2$. Figure 7 shows the temperature dependence of HF for Sr_2FeO_3 together with $SrFeO_2$ and $Sr_3Fe_2O_5$, where the temperature is normalized, for comparison, by T_N. The HF evolves in the same way down to low temperatures, independent of dimensionality. We fitted the HF

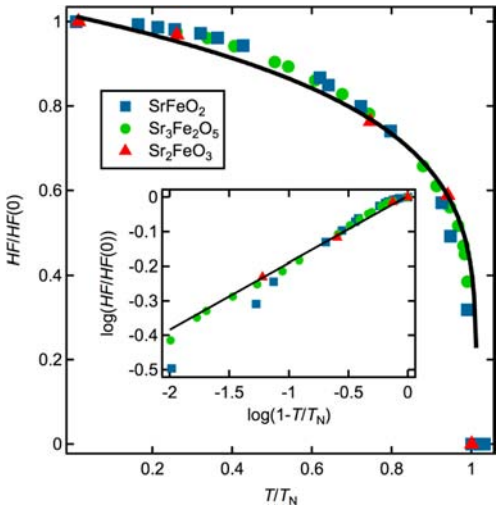

Figure 7. Evolution of the hyperfine field of Sr_2FeO_3 against temperature. Inset shows a log−log plot of $HF(T)/HF(0)$ vs $(1 - T/T_N)$. The black lines show computational fitting of $HF(T)/HF(0) \propto (1 - T/T_N)^\beta$.

versus T curve using a power law of the form $HF(T)/HF(0) \propto (1 - T/T_N)^\beta$ (see the inset of Figure 7). Fitting in a range of $0.2 < T/T_N < 1$, we obtained T_N = 179(5) K, β = 0.186(27) for Sr_2FeO_3. The obtained value of β is comparable with β = 0.26 and β = 0.22 for $SrFeO_2$ and $Sr_3Fe_2O_5$, respectively.[22] The similar temperature dependence of the ordered moment for n = 1, 2, ∞ might indicate the dimensionality is solely scaled by T_N. Note that β obtained here is not a critical exponent to determine universality classes.

It is interesting to compare $Sr_{n+1}Fe_nO_{2n+1}$ with $Sr_3Fe_2O_4Cl_2$ recently discovered by Hayward and co-workers.[20] This material exhibits the same spin structure as $Sr_3Fe_2O_5$, and its T_N is 378 K. Both $Sr_3Fe_2O_4Cl_2$ and $Sr_3Fe_2O_5$ have a double-layered structure, but the former structure has double square-lattice ($J_{\|}$) layers bridged by $J_\perp$ (see Figure 1e). Each iron in $Sr_3Fe_2O_4Cl_2$ is connected by four $J_{\|}$'s and one $J_\perp$, while that in $Sr_3Fe_2O_5$ is connected by three $J_{\|}$'s and two $J_\perp$'s. $SrFeO_2$ has four $J_{\|}$'s and two $J_\perp$'s. Having $J_{\|} > J_\perp$, it is reasonably understood that the T_N of $Sr_3Fe_2O_4Cl_2$ is located between $Sr_3Fe_2O_5$ and $SrFeO_2$.

It is also informative to address the magnetism of Sr_2FeO_3 with the isostructural compound Sr_2CuO_3. Sr_2CuO_3 has only one active orbital (i.e., x^2-y^2), forming the Cu−O−Cu superexchange interaction ($J_{\|}$ = 2200 K).[23] The face-to-face Cu−Cu interaction ($J_\perp$) is negligibly small. This makes Sr_2CuO_3 an S = 1/2 quasi 1D chain system. The extremely low Néel temperature (~ 5 K) relative to the intrachain interaction is understood in terms of the quantum nature of spins as well as the good one-dimensionality.

Results of Mössbauer spectroscopy and neutron diffraction demonstrate that, like the other two members, Sr_2FeO_3 displays the same spin orientation with the magnetic moments lying parallel to the square plane. More specifically, the magnetic moments for Sr_2FeO_3 and $Sr_3Fe_2O_5$ point parallel to c (the chain and leg direction) and not parallel to b. According to Koo et al. who performed GGA+U+SOC calculations[9] for $Sr_3Fe_2O_5$, the stabilized c axis orientation (vs the b axis) is due to a wider $yx\downarrow$ band (vs $zx\downarrow$), where x, y, and z correspond, respectively, to a, b, and c. Because of the absence of the rung coupling (namely, Fe−O−Fe bonding along c) for Sr_2FeO_3, the $zx\downarrow$

dx.doi.org/10.1021/ic400444u | Inorg. Chem. 2013, 52, 6096−6102

band should be narrower than that of $SrFe_2O_5$, while keeping the $yx\downarrow$ bandwidth.

Although the present study is concerned with the intermediate dimensional magnetism of insulators, it can serve for itinerant magnetism too. We recently demonstrated that the A_2BO_3 structures like Sr_2CuO_3 in general exhibit a structural transition under high pressure that involves a phase shift of the AO_4 stacked chain blocks.[24] Sr_2FeO_3 could be an interesting compound for the observation of such transition. Furthermore, $SrFeO_2$ and $Sr_3Fe_2O_5$ undergo three transitions simultaneously at around 34 GPa: a spin-state transition, an insulator−metal (I-M) transition, and an antiferro-to-ferromagnetic (AF-F) transition.[25] It is shown that the minimal unit for spin state transition is the two face-to-face FeO_4 square planes, and the interplane distance defines the critical pressure. Therefore, Sr_2FeO_3 would also exhibit a spin-state transition from high spin state to intermediate spin state at around 34 GPa. However, whether or not the pressure-induced spin transition involves I-M and/or AF-F transitions is not obvious. For instance, spin fluctuations enhanced because of the reduced dimensionality in Sr_2FeO_3 may have a significant influence on the electronic structures as well as the stability of spin order pattern.

CONCLUSION

Sr_2FeO_3 was synthesized by the low temperature reaction of Sr_2FeO_4 with CaH_2. The structure shows square-planar coordinate irons sharing corners and forming unidirectional infinite chains running parallel to each other. Sr_2FeO_3 is isostructural with Sr_2CuO_3 (*Immm* space group) and is the n = 1 member of the serial lattice system $Sr_{n+1}Fe_nO_{2n+1}$. $Sr_{n+1}Fe_nO_{2n+1}$ is a unique system connecting between 2D and 3D. The *G*-type AF order was observed in this material below 179 K. Compared to other existing compounds, that is, $SrFeO_2$ (n = ∞; T_N = 468 K) and $Sr_3Fe_2O_5$ (n = 2; T_N = 296 K), Sr_2FeO_3 has the lowest magnetic order because of the unidirectional loss of the $J_{\|}$ superexchange interaction. However, the temperature dependence of the magnetic moment shows a universal behavior. Owing to the two-dimensionality, spin dynamics involving short-range ordering might be present. Thus, NMR and μSR study would be highly interesting.

ASSOCIATED CONTENT

Supporting Information

Further details are given in Figures S1−S5 and Table S1. This material is available free of charge via the Internet at http://pubs.acs.org.

AUTHOR INFORMATION

Corresponding Author

*E-mail: kage@scl.kyoto-u.ac.jp.

Notes

The authors declare no competing financial interest.

ACKNOWLEDGMENTS

The authors would like to thank Dr. Atsushi Kitada and Dr. Takeshi Yajima for their help during the neutron measurements. This work was supported by CREST.

REFERENCES

(1) Hase, M.; Terasaki, I.; Uchinokura, K. *Phys. Rev. Lett.* **1993**, *70*, 3651.
(2) Haldane, F. D. M. *Phys. Rev. Lett.* **1983**, *50*, 1153.
(3) Misguich, G.; Lhuillier, C. *Frustrated Spin Systems*; World Scientific: Singapore, 2005.
(4) (a) Kodama, K.; Takigawa, M.; Horvatić, M.; Berthier, C.; Kageyama, H.; Ueda, Y.; Miyahara, S.; Becca, F.; Mila, F. *Science* **2002**, *298*, 395. (b) Onizuka, K.; Kageyama, H.; Narumi, Y.; Kindo, K.; Ueda, Y.; Goto, T. *J. Phys. Soc. Jpn.* **2000**, *69*, 1016.
(5) Dagotto, E.; Rice, T. M. *Science* **1996**, *271*, 618.
(6) Hiroi, Z.; Takano, M.; Azuma, M.; Takeda, Y. *Nature* **1993**, *364*, 315.
(7) (a) Tsujimoto, Y.; Tassel, C.; Hayashi, N.; Watanabe, T.; Kageyama, H.; Yoshimura, K.; Takano, M.; Ceretti, M.; Ritter, C.; Paulus, W. *Nature* **2007**, *450*, 1062. (b) Kageyama, H.; Watanabe, T.; Tsujimoto, Y.; Kitada, A.; Sumida, Y.; Kanamori, K.; Yoshimura, K.; Hayashi, N.; Muranaka, S.; Takano, M.; Ceretti, M.; Paulus, W.; Ritter, C.; André, G. *Angew. Chem., Int. Ed.* **2008**, *47*, 5740. (c) Tassel, C.; Kageyama, H. *Chem. Soc. Rev.* **2012**, *41*, 2025.
(8) Xiang, H. J.; Wei, S.-H.; Whangbo, M. H. *Phys. Rev. Lett.* **2008**, *100*, 167207.
(9) Koo, H. J.; Xiang, H.; Lee, C.; Whangbo, M. H. *Inorg. Chem.* **2009**, *48*, 9051.
(10) Tomiyasu, K.; Kageyama, H.; Lee, C.; Whangbo, M. H.; Tsujimoto, Y.; Yoshimura, K.; Taylor, W. J.; Lobet, A.; Trouw, F.; Kakurai, K.; Yamada, K. *J. Phys. Soc. Jpn.* **2010**, *79*, 034707.
(11) Teske, C. L.; Mueller-Buschbaum, H. *Z. Anorg. Allg. Chem.* **1970**, *379*, 234.
(12) Petricek, V.; Dusek, M.; Palatinus, L. *Jana2006, The crystallographic computing system*; Institure of Physics: Praha, Czech Republic, 2006.
(13) Izumi, F.; Momma, K. *Solid State Phenom.* **2007**, *130*, 15.
(14) Brown, I. D.; Altermatt, D. *Acta Crystallogr., Sect. B* **1985**, *41*, 244.
(15) Dann, S. E.; Weller, M. T.; Currie, D. B. *J. Solid State Chem.* **1991**, *92*, 237.
(16) Pelloquin, D.; Hadermann, J.; Giot, M.; Caignaert, V.; Michel, C.; Hervieu, M.; Raveau, B. *Chem. Mater.* **2004**, *16*, 1715.
(17) Stephens, P. *J. Appl. Crystallogr.* **1999**, *32*, 281.
(18) Dann, S. E.; Weller, M. T.; Currie, D. B.; Thomas, M. F.; Al-Rawwas, A. D. *J. Mater. Chem.* **1993**, *3*, 1231.
(19) (a) Tassel, C.; Watanabe, T.; Tsujimoto, Y.; Hayashi, N.; Kitada, A.; Sumida, Y.; Yamamoto, T.; Kageyama, H.; Takano, M.; Yoshimura, K. *J. Am. Chem. Soc.* **2008**, *130*, 3764. (b) Tassel, C.; Pruneda, J. M.; Hayashi, N.; Watanabe, T.; Kitada, A.; Tsujimoto, Y.; Kageyama, H.; Yoshimura, K.; Takano, M.; Nishi, M.; Ohoyama, K.; Mizumaki, M.; Kawamura, N.; Íñiguez, J.; Canadell, E. *J. Am. Chem. Soc.* **2009**, *131*, 221.
(20) Dixon, E.; Hayward, M. A. *Inorg. Chem.* **2010**, *49*, 9649.
(21) Bridges, C. A.; Darling, G. R.; Hayward, M. A.; Rosseinsky, M. J. *J. Am. Chem. Soc.* **2005**, *127*, 5996.
(22) Hayashi, N.; Kageyama, H.; Tsujimoto, Y.; Watanabe, T.; Muranaka, S.; Ono, T.; Nasu, S.; Ajiro, Y.; Yoshimura, K.; Takano, M. *J. Phys. Soc. Jpn.* **2010**, *79*, 123709.
(23) Motoyama, N.; Eisaki, H.; Uchida, S. *Phys. Rev. Lett.* **1996**, *76*, 3212.
(24) Yamamoto, T.; Kobayashi, Y.; Okada, T.; Yagi, T.; Kawakami, T.; Tassel, C.; Kawasaki, S.; Abe, N.; Niwa, K.; Kikegawa, T.; Hirao, N.; Takano, M.; Kageyama, H. *Inorg. Chem.* **2011**, *50*, 11787.
(25) (a) Yamamoto, T.; Tassel, C. d.; Kobayashi, Y.; Kawakami, T.; Okada, T.; Yagi, T.; Yoshida, H.; Kamatani, T.; Watanabe, Y.; Kikegawa, T.; Takano, M.; Yoshimura, K.; Kageyama, H. *J. Am. Chem. Soc.* **2011**, 6036. (b) Kawakami, T.; Tsujimoto, Y.; Kageyama, H.; Chen, X. Q.; Fu, C. L.; Tassel, C.; Kitada, A.; Suto, S.; Hirama, K.; Sekiya, Y.; Makino, Y.; Okada, T.; Yagi, T.; Hayashi, N.; Yoshimura, K.; Nasu, S.; Podloucky, R.; Takano, M. *Nat. Chem.* **2009**, *1*, 371.